

Article

Not peer-reviewed version

Simultaneously Recovery of Thorium and Tungsten by Hybrid Electrolysis–Nanofiltration Processes

Geani Teodor Man , [Paul Constantin Albu](#) , [Aurelia Cristina Nechifor](#) , [Alexandra Raluca Grosu](#) ,
Diana Ionela Popescu (Stegarus) , [Vlad-Alexandru Grosu](#) ^{*} , Virgil Emanuel Marinescu , [Gheorghe Nechifor](#) ^{*}

Posted Date: 19 December 2023

doi: 10.20944/preprints202312.1375.v1

Keywords: thorium recovery; wolfram recovery; membrane processes; membrane electrolysis; nanofiltration; thorium recycling; wolfram recycling; Pourbaix diagrams



Preprints.org is a free multidiscipline platform providing preprint service that is dedicated to making early versions of research outputs permanently available and citable. Preprints posted at Preprints.org appear in Web of Science, Crossref, Google Scholar, Scilit, Europe PMC.

Copyright: This is an open access article distributed under the Creative Commons Attribution License which permits unrestricted use, distribution, and reproduction in any medium, provided the original work is properly cited.

Article

Simultaneously Recovery of Thorium and Tungsten by Hybrid Electrolysis–Nanofiltration Processes

Geani Teodor Man ^{1,2}, Paul Constantin Albu ³, Aurelia Cristina Nechifor ¹,
Alexandra Raluca Grosu ¹, Diana Ionela Popescu (Stegarus) ², Vlad-Alexandru Grosu ^{4,*},
Virgil Emanuel Marinescu ⁵ and Gheorghe Nechifor ^{1,*}

¹ Analytical Chemistry and Environmental Engineering Department, University Politehnica of Bucharest, 011061 Bucharest, Romania; man_geani@yahoo.com (G.T.M.); aureliacristinanechifor@gmail.com (A.C.N.); andra.grosu@upb.ro (A.R.G.); gheorghe.nechifor@upb.ro (G.N.)

² National Research and Development Institute for Cryogenics and Isotopic Technologies–ICSI, 240050 Râmnicu Valcea, Romania; geani.man@icsi.ro (G.T.M.); stegarus@icsi.ro (D.I.P.)

³ Radioisotopes and Radiation Metrology Department (DRMR), IFIN Horia Hulubei, 023465 Măgurele, Romania; paulalbu@gmail.com (P.C.A.);

⁴ Department of Electronic Technology and Reliability, Faculty of Electronics, Telecommunications and Information Technology, University Politehnica of Bucharest, 061071 Bucharest, Romania; vlad.grosu@upb.ro (V.-A.G.)

⁵ Department of Physical-chemical tests, National Institute for Research and Development in Electrical Engineering ICPE–CA Bucharest, 030138 Bucharest, Romania; virgil.marinescu@icpe-ca.ro (V.E.M.)

* Correspondence: vlad.grosu@upb.ro (V.-A.G.); ghnechifor@gmail.com (G.N.)

Abstract: The recovery and recycling of metals that generate toxic ions in the environment is of particular importance, especially when these are tungsten and, in particular, thorium. The radioactive element thorium has unexpectedly accessible domestic applications (filaments of light bulbs and electronic tubes, welding electrodes, working alloys containing aluminum and magnesium), which lead to its appearance in electrical and electronic waste from municipal waste management platforms. The current paper proposes the simultaneous recovery of waste containing tungsten and thorium from welding electrodes. The simultaneous recovery is done by applying a hybrid membrane electrolysis technology coupled with nanofiltration. An electrolysis cell with sulphonated polyether–ether–ketone membranes (sPEEK) and a nanofiltration module with chitosan-polypropylene membranes (C–PHF–M) are used to carry out the hybrid process. The analysis of welding electrodes led to a composition of: W (tungsten) 89.4%; Th 7.1%; O₂ 2.5% and Al 1.1%. Thus, the parameters of the electrolysis process were chosen according to the speciation of the three metals suggested by the superimposed Pourbaix diagrams. At a constant potential of 20.0 V and an electrolysis current of 1.0 A, the pH is varied and the possible composition of the solution in the anodic workspace is analyzed. Favorable conditions for both electrolysis and nanofiltration were obtained at pH from 6 to 9, when the soluble tungstate ion, the aluminum hydroxide and solid thorium dioxide were formed. Through a first nanofiltration, the tungstate ion is obtained in the permeate, and thorium dioxide and aluminum hydroxide in the concentrate. By adding a pH 13 solution over the two precipitates, the aluminum is solubilized as sodium aluminate which will be found after the second nanofiltration in permeate, the thorium dioxide remaining integrally (within an error of ± 0.1 ppm) on the C–PHF–M membrane.

Keywords: thorium recovery; wolfram recovery; membrane processes; membrane electrolysis; nanofiltration; thorium recycling; wolfram recycling; Pourbaix diagrams

1. Introduction

The performances proven by membrane separation processes in various ecological and greening technologies constitute the important arguments for their involvement in the recovery and recycling of various urban wastes, especially those that generate toxic products [1–4]. Thus, in order to develop a technology for the separation and valorization of some metallic elements from specific urban waste, baromembrane processes can be approached, when the elements are in colloidal (nanometric) or

suspension (micrometric) state, or processes with electric and/or concentration gradient, if the metals are found in the forms of ions [5–8].

The development of new technologies for the recovery of metals from urban waste requires solid arguments regarding the value of the separated metals or the negative impact on the environment if such metals are not separated and recycled [9–11]. A special case, reported recently [12], shows that metals such thorium or tungsten that come from electric and electronic equipment or materials used in construction (refractory bricks, welding electrodes) can appear in the urban waste [13,14]. The recovery of both metals is of technical importance because they have high practical utility (Figure 1) [11,15], but also because they have a particularly undesirable impact on the environment, especially thorium [16].

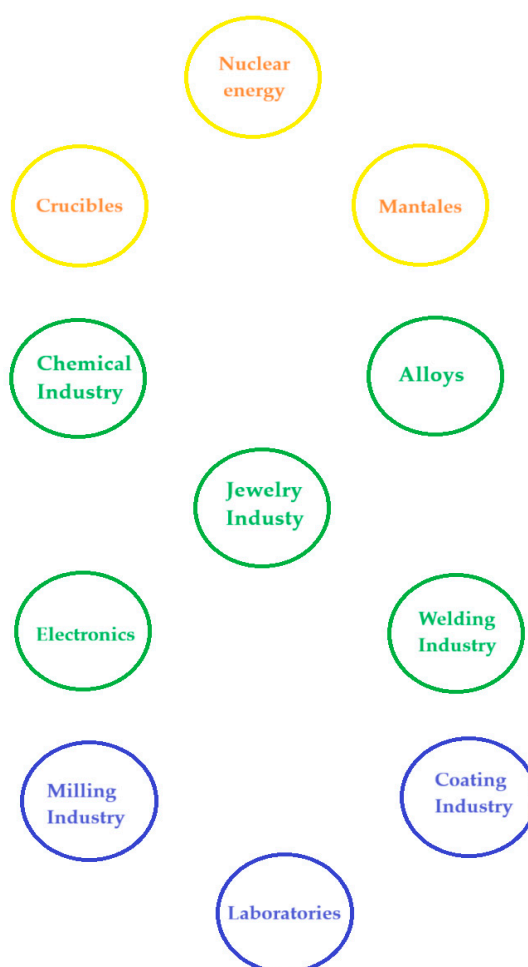


Figure 1. Some of the individual and common applications of tungsten and thorium: (blue) tungsten; (yellow) thorium; (green) common.

Both thorium and tungsten are obtained from ores by established processes such as: hydrometallurgical [17–19], separation [20–24], treatment of alloys [25]. Moreover, tungsten has been the focus of process engineers for its recovery from various residues through electrolytic processes, acid or basic solubilization processes [26–30]. On the other hand, thorium has been the focus of researchers in the field of membranes, for concentration, separation or purification, especially when it comes from ores in which uranium or rare earths can also be found [31–39].

This work studies the simultaneous recovery of tungsten and thorium, from waste coming from the welding industry with W–Th electrodes, through a hybrid technology of membrane electrolysis and nanofiltration. The membrane used in the electrolysis cell is based on sulfonated polyether–

ether-ketone (sPEEK-M), and the membrane used for nanofiltration is chitosan deposited on propylene hollow fiber (C-PHF-M).

2. Materials and Methods

2.1. Reagents and Materials

All reagents and organic compounds used in the presented work were of analytical grade. Th(NO₃)₄·5H₂O, KSCN, NaCl, NaOH pellets, Ca(OH)₂, HNO₃ (68%), H₂SO₄ (96%), HCl 35% suprapure and NH₄OH 25% (analytical grade) were purchased from Merck KGaA Darmstadt, Germany.

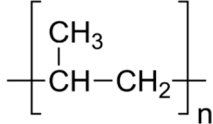
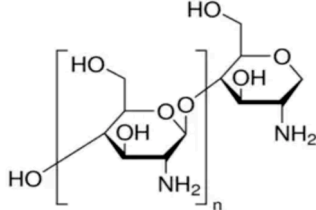
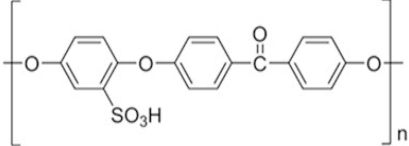
Aluminon, Torin and glacial acetic acid (analytical grade, Sigma-Aldrich Chemie GmbH, Steinheim, Germany) were used in the studies.

Materials: polyether-ether-ketone (PEEK), Mw=30,000 g/mol, q=1.24 g/cm³ powder, average particle size 80 micron; chitosan, high molecular weight, (Merck KGaA, Darmstadt, Germany), red band welding electrodes (ProConstruct Distribution SRL, Balotești, Romania).

The hollow fibers polypropylene support membranes (PHF-M) were provided by GOST Ltd., Perugia, Italy [40,41].

The purified water characterized by 18.2 μS/cm conductivity was obtained with a RO Millipore system (MilliQ® Direct 8 RO Water Purification System, Merck, Darmstadt, Germany).

Table 1. The characteristics of the used polymer compounds.

Organic Compounds	Name and Symbol	Molar mass (g/mol)	Solubility (g/L)	pKa
	Polypropylene (PP)	–	–	7.0
	Chitosan (Chi)	High molecular weight	soluble in acid media (0.5 M HCl: 50 mg/mL)	6.2 to 7.0
	sulfonated polyether-ether-ketone (sPEEK)	35,000	organic polar solvents	2.0 to 2.2

2.2. Procedures and methods

2.2.1. Preparation of sPEEK-M membranes from PEEK solution in sulfuric acid

In a conical glass of 250 cm³, introduce 30 mL H₂SO₄ of concentration 96%, after which 2.5 g polymer is gradually added, stirring continuously with a glass rod to avoid agglomeration of the polymer. After about 2 hours of stirring, the glass is covered with a thin layer of parafilm and is kept without stirring for up to 48 hours from the moment of covering the solution, to favor the complete dissolution of the polymer in acid. In this time interval the sulfonation of the polymer occurs. A clear brick-colored solution with a concentration of approx. 4.5% PEEK is obtained. In order to obtain the actual support membranes, the polymer solution is introduced for gelation and washing in 300 mL of water, in portions of 100 mL each, separated and applied on a spectral glass plate with the help of

a chromatographic scraper knife having slit opening between 0.5 and 0.6 mm. The pellicle is dried at 60 °C for 2 hours, is washed well with distilled water and placed in a $\text{Ca}(\text{OH})_2$ bath where it is kept for 48 hours, then removed and washed repeatedly in ultrapure water (Figure 2). The removal of the sulfate ion was followed by the identification reaction with a 2 mol/L barium chloride solution. The main macroscopic observations, which can be highlighted, in the case of incomplete washing are [42,43]:

- undulation of the membrane;
- the occurrence of defects (microcracks, holes);
- local re-solubilizations (transparencies, gelations).



Figure 2. Preparation of sPEEK-M membranes from PEEK solution in sulfuric acid.

sPEEK-M membranes were characterized by scanning electron microscopy (SEM) and Energy Dispersive X-ray Spectroscopy (EDAX).

2.2.2. Preparation of Chitosan-Polypropylene Hollow Fibers membranes (C-PHF-M)

In a round-bottomed flask, a chitosan solution is prepared under continuous magnetic stirring by dissolving 10 g of chitosan powder in 990 mL of 10% acetic acid solution. After mixing for about two hours, a yellowish-white solution is obtained, which is the feed phase of the ultrafiltration membrane module (Figure 3) equipped with polypropylene hollow fiber membrane. With the help of a recirculation pump, a pressure of 6 bars is ensured in the space between the body of the module and the outside of the membranes, in a closed circuit. The permeate, which is made up of the acetic acid solution, is collected inside the membranes. A layer of chitosan is deposited on the polypropylene hollow fiber membrane [44,45].

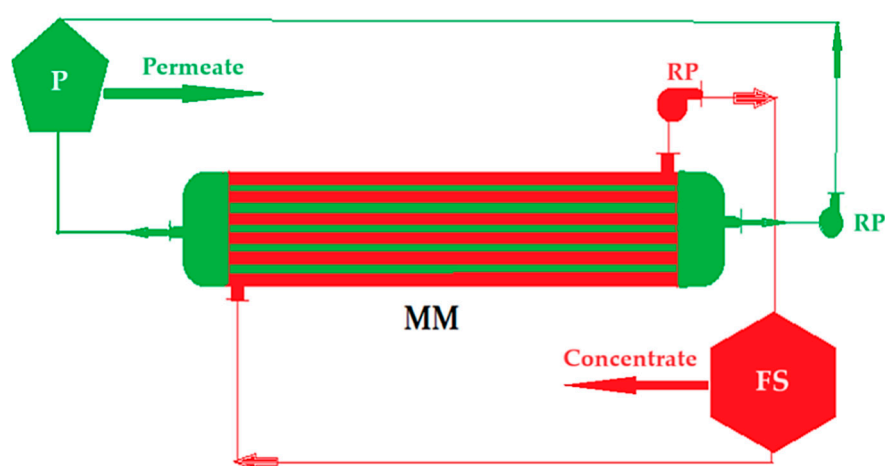


Figure 3. Schematic of the nanofiltration installation for the preparation of C-PHF-M membrane: MM – membrane module; P – permeate; FS – feed solution; RP – recirculation pumps.

The C-PHF-M membranes were characterized by scanning electron microscopy (SEM), Energy Dispersive X-ray Spectroscopy (EDAX) and from the perspective of performance in the nanofiltration process.

2.2.3. Electrolysis of tungsten and thorium-based electrodes in acidic aqueous solution

250 mL volume of each solution was introduced, in turn, into an electrolysis cell (Figure 4) of the MASTECH HY3005D-3 potentiostat equipment provided with three electrodes: tungsten welding electrode as anode, platinum wire as cathode, and a reference electrode. The potentiostat was operated at a potential of +20.0 V and an electrolysis current of 1.0 A. The pH in the anodic space was imposed at 0, 2, 4, 6, 8 and 10, 12, and in the cathodic space at pH 13, using hydrochloric acid and sodium hydroxide, respectively. The experimental procedure took place at room temperature. After six hours of work at the cell base, both solutions (anodic and cathodic) were collected, and subjected to nanofiltration in order to recover of thorium as thorium dioxide and tungsten as tungstate ion. The chloride anion concentration was followed up with a combined selective chloride electrode (HI 4107, Hanna Instruments Ltd., Leighton Buzzard, UK) and a multiparameter system (HI 5522, Hanna Instruments Ltd., Leighton Buzzard, UK).

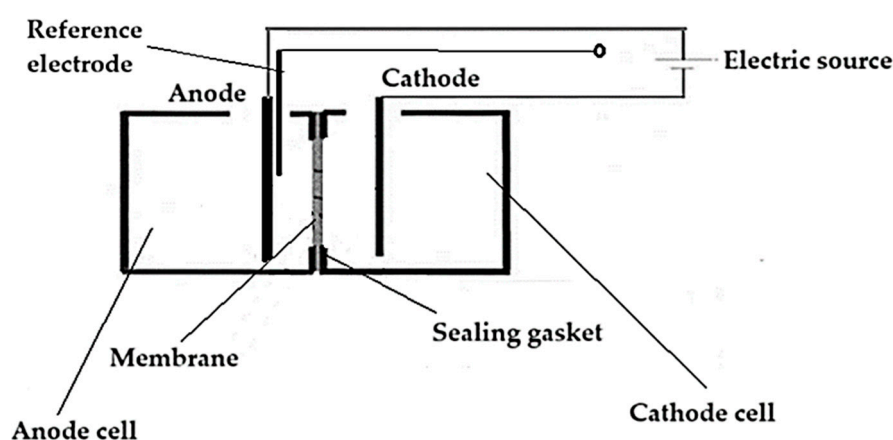


Figure 4. The schema of the electrolysis cell of tungsten electrodes for the recovery of thorium, and tungsten.

For the recovery of thorium dioxide, both the solution from the anodic space and the one from the cathode space are nanofiltered, both of which constitute the feed solutions (FS) of the membrane mode in the installation diagram in Figure 3. This time the module is equipped with a chitosan-polypropylene nanofiltration membrane. A separate module is used for each of the two feeding solutions, so that the components in the anodic and cathodic space can be identified.

2.3. Equipment

The membranes microscopy studies, SEM and HFSEM, were performed on a Hitachi S4500 system (Hitachi High-Technologies Europe GmbH, Germany) [46].

The UV-Vis analyses of the solutions were done on a Spectrometer CamSpec M550 (Spectronic CamSpec Ltd., Leeds, UK) [47].

The UV-Vis studies on the nanoparticles samples composition were performed on dual-beam UV equipment – Varian Cary 50 (Agilent Technologies Inc., Santa Clara, California, USA) at a resolution of 1 nm, spectral bandwidth 1.5 nm, and 300 nm/s scan rate. The UV-Vis spectra of the samples were recorded for a wavelength from 200 to 800 nm, at room temperature, using 10 mm quartz cells [48].

MASTECH HY3005D-3 (San Jose, CA, USA) is a working power supply which has an electrical output, continuously adjustable, between 0–30 V DC and 0–5 A.

The validation of the electrochemical processes was followed up with a PARSTAT 2273 Potentiostat (Princeton Applied Research, AMETEK Inc., USA). A glass cell with three electrodes setup was used [47,48].

The pH of the medium was followed up with a combined selective electrode (HI 4107, Hanna Instruments Ltd, UK) and a multiparameter system (HI5522, Hanna Instruments Ltd, Leighton Buzzard, UK) [49].

To assess and validate the content in metal ions, the atomic absorption spectrometer AAnalyst 400 AA Spectrometer (Perkin Elmer Inc., Waltham, Massachusetts, USA) with WinLab32-AA software (Perkin Elmer Inc., Waltham, Massachusetts, USA), with a single-element hollow-cathode lamp was used [50].

In the case of the present work, for the validation of the SEM and EDAX analyses, the tungsten electrodes samples subjected to the analysis were visualized with the help of the FESEM-FIB workstation (scanning electron microscope with field emission electron and focused beam of ions) model Auriga (Carl Zeiss SMT, Oberkochen, Germany), by means of the secondary electron/ion detector (SESI) in the sample chamber for the topography/morphology of the surface of the analyzed samples [51].

The verification of the chemical composition was carried out with the help of the EDS probe (energy dispersive spectrum for the characteristic X-ray) produced by Oxford Instruments, UK – energy dispersive spectrometer model X-MaxN with the Aztec acquisition and processing software integrated on the FESEM-FIB Auriga working station [52].

Secondary electron (SE) topography images were acquired and analyzed from the sample chamber with the Everhart Thornley SESI secondary electron detector with Faraday cup (SESI)/in-column annular SE in-lens detector, at a voltage acceleration of 5 kV for sample visualization and 10 kV for EDS spectroscopy, for the following types of analyzes carried out by the energy dispersive probe, on the surface of the analyzed sample:

- semi-quantitative spot analyses located at certain intervals in the same micro-area, for the distribution of elements from the point of view of composition on the surface of the material as well as the variational verification of the composition of the investigated micro-area with the points from which the respective spectra were acquired;
- elemental mapping analyses, i.e. obtaining spectral images – where the distribution of the elements on the surface swept by the electron beam is superimposed and possible compositional differences are highlighted – increasing the area of the present element or the appearance/disappearance of an analyzed and identified element.

3. Results and discussion

The interest in thorium is argued both because it is a material with huge potential for energy generation, including the nuclear energy [53] but also because, although it is radioactive, it is the object of some domestic applications that capitalize on the resistance to high temperatures of thorium dioxide (lamps, shields, crucibles, welding electrodes) [54] or special refractive index (lenses, glasses, high resolution opto-electronic apparatus) [12]. It becomes obvious that, with the use of these materials, but also because thorium has a natural abundance similar to that of lead [55] it will be found in urban industrial waste arriving in various forms on municipal integrated processing platforms [56].

In this paper, the possibility of recovering thorium from waste from the welding industry is studied based on a hybrid technology consisting of membrane electrolysis coupled with nanofiltration.

3.1. Characterization of the sPEEK-M membrane

Membranes of sulfonated polyether-ether-ketone (sPEEK) [42,43] or sPEEK polymer composites [44] are used in ultrafiltration, nanofiltration or reverse osmosis processes [42,45]. To carry out the electrolysis process of the tungsten electrodes, a specific sPEEK cation exchange membrane was prepared by forming it from sulfonated polyether-ether-ketone gel, drying in a vacuum oven at 60 °C for 2 hours and fixing in a bath with calcium hydroxide solution. Here it is kept for 48 hours, then it is removed and washed repeatedly in ultrapure water. Three samples of 1 cm² each from the membrane obtained after fixing with calcium hydroxide and after keeping in

ultrapure water are introduced in a Dewar vessel with liquid nitrogen, and fractured. After coating with a superficial layer (50 nm) of gold, the membrane obtained from the fixing bath with calcium hydroxide (Figures 5 and 6) and the one obtained after washing and keeping in pure water (Figures 7 and 8) are SEM and EDAX characterized.

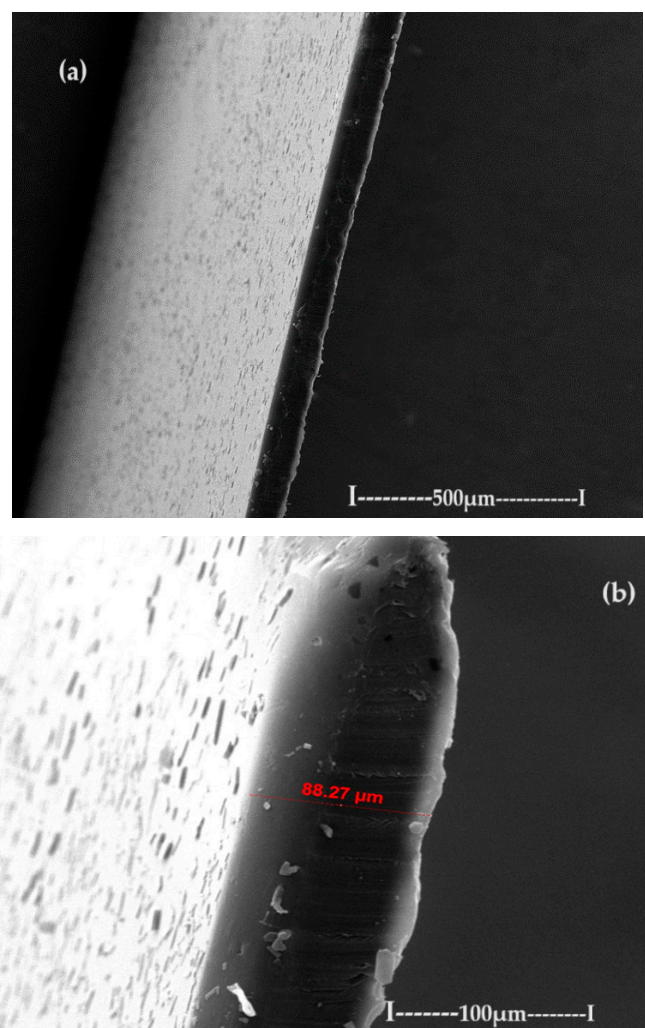


Figure 5. The images obtained by scanning electron microscopy (SEM) for: (a) the section of the membrane after keeping it in the calcium hydroxide bath; and (b) the detail of the section.

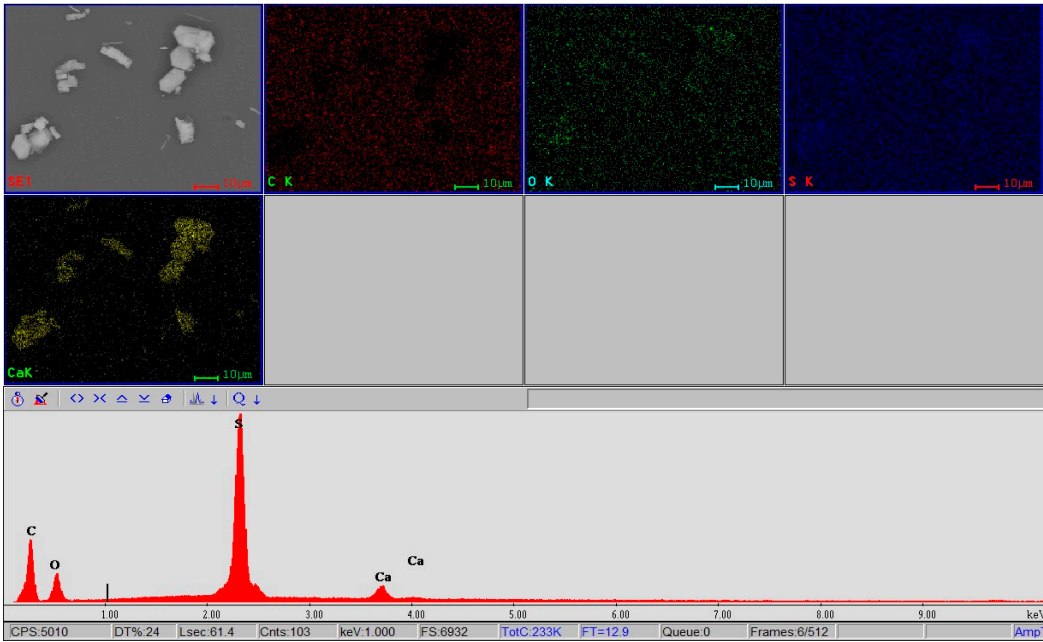


Figure 6. Energy Dispersive X-ray Spectroscopy (EDAX) of the membrane after keeping it in the calcium hydroxide bath.

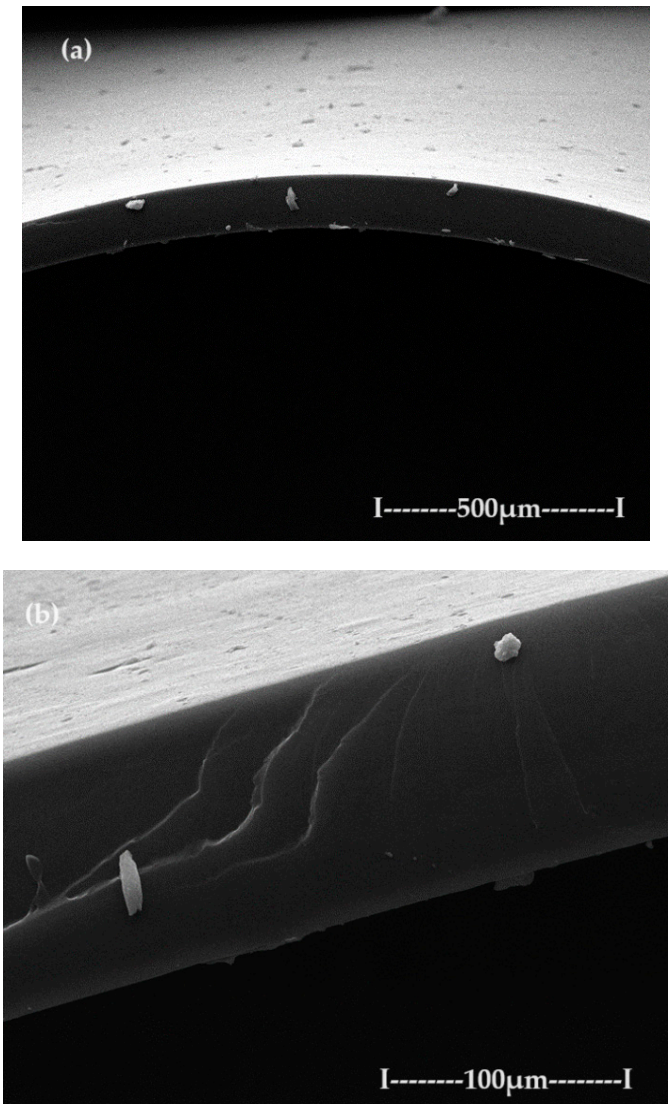


Figure 7. The image obtained by scanning electron microscopy (SEM) for: (a) section of the washed membrane; and (b) the detail of the section.

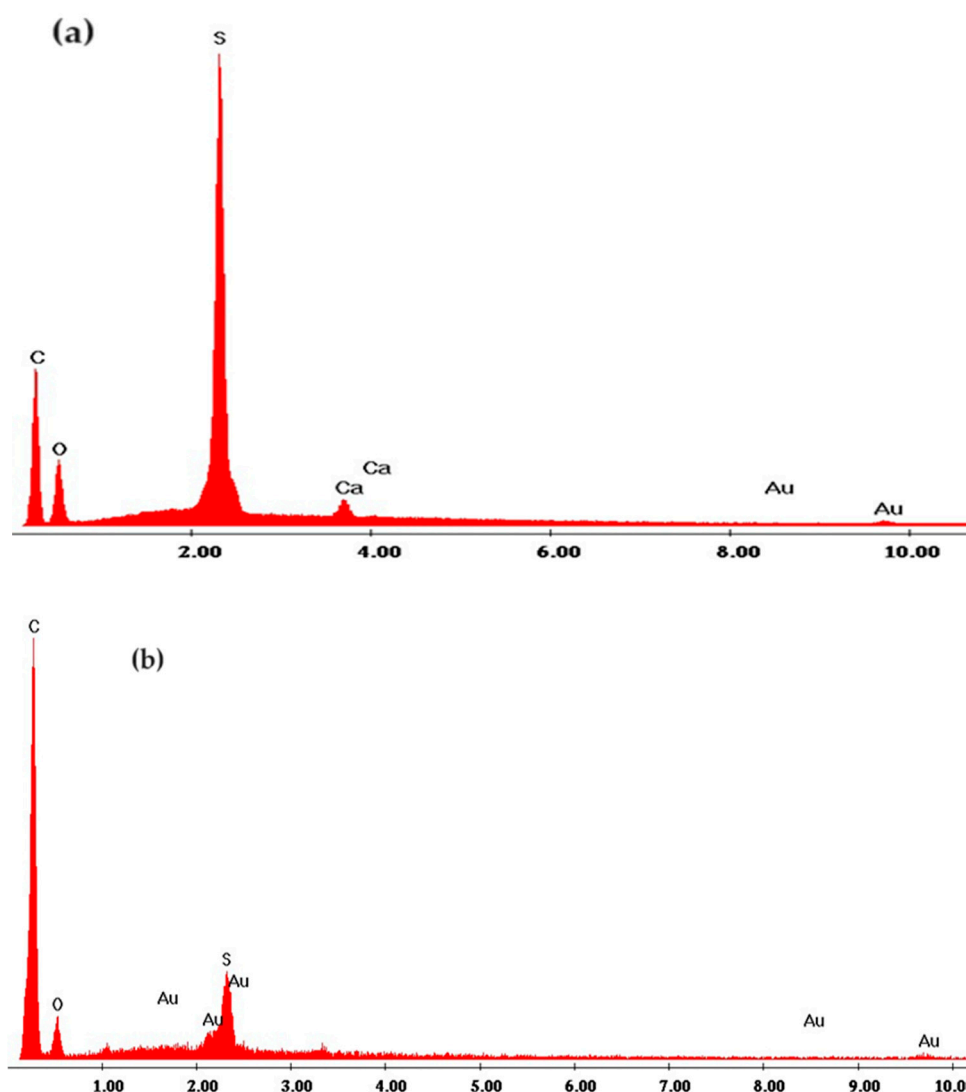


Figure 8. Comparative Energy Dispersive X-ray Spectroscopy (EDAX): (a) membrane before washing; and (b) membrane after keeping in ultrapure water.

3.2. Characterization of C-PHF-M membrane

The membranes based on chitosan have been frequently used to carry out membrane processes for the separation of ions and molecules [57–60], but in this work chitosan membranes are obtained on a polypropylene hollow fiber (C-PHF-M) support. Practically, the polypropylene hollow fiber (PHF) support, which has previously presented ultrafiltration performances [43–45], is transformed in nanofiltration composite membranes (C-PHF-M) by ultrafiltration of a chitosan solution to obtain *in situ* a selective layer of chitosan. Samples of 3 cm polypropylene hollow fiber membrane and chitosan-polypropylene hollow fiber membrane were fractured in liquid nitrogen and covered with a superficial layer (50 nm) of gold and characterized by scanning electron microscopy (SEM) (Figures 9 and 10).

The support membrane (Figure 9a) with pores of 0.002–0.2 μm specific for micro and ultrafiltration is transformed after the coating with chitosan (Figure 9b) into the composite membrane (C-PHF-M) for nanofiltration with pores smaller than 0.002 μm .

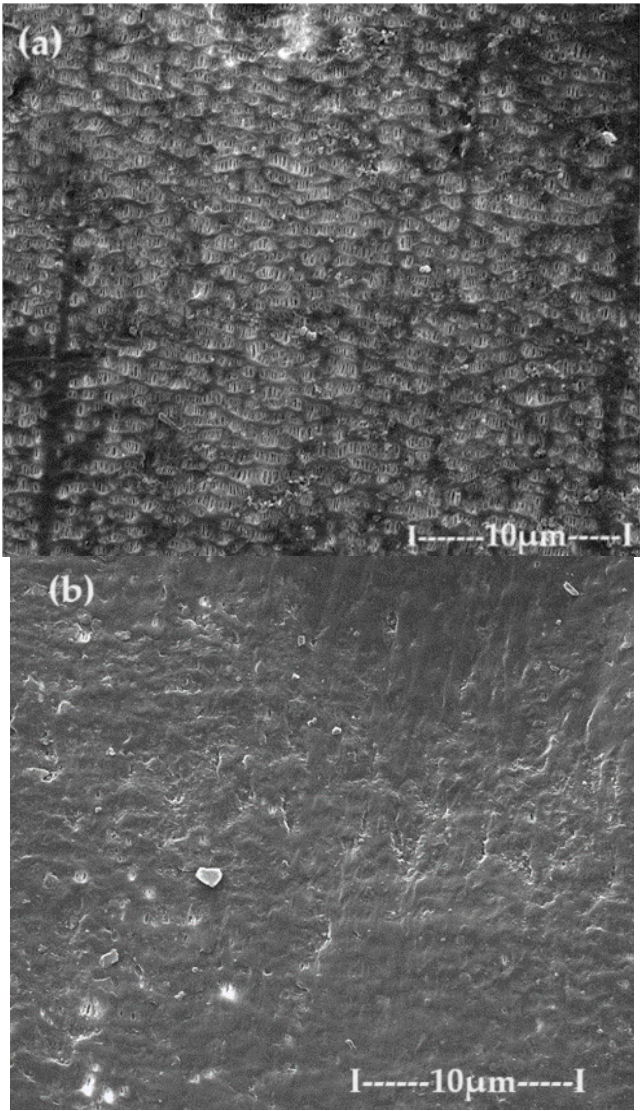


Figure 9. The image obtained by scanning electron microscopy (SEM) for: **(a)** polypropylene hollow fiber membrane (PHF-M) surface; **(b)** chitosan-polypropylene hollow fiber membrane (C-PHF-M).

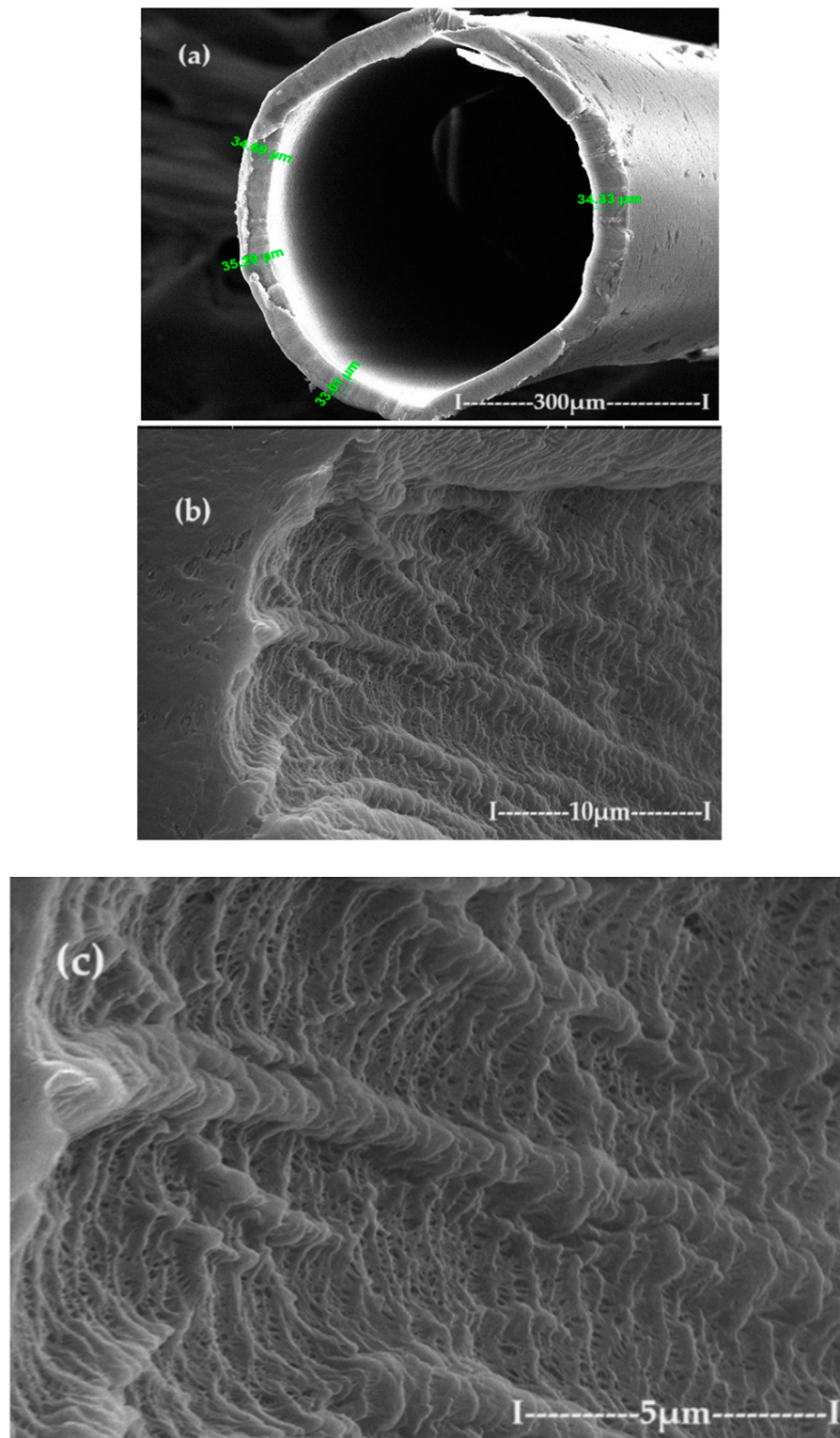


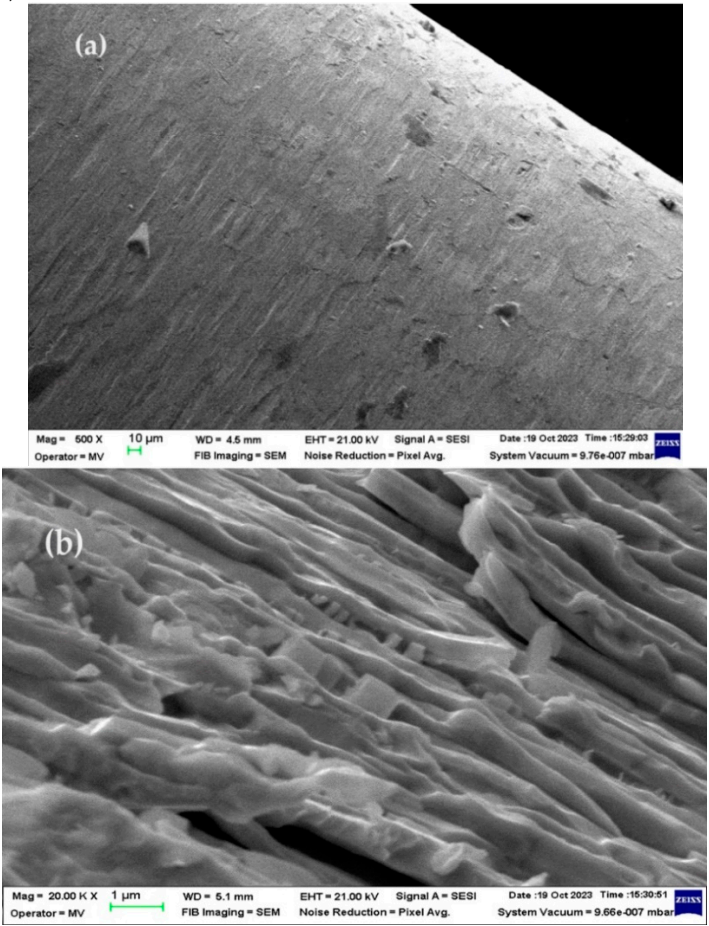
Figure 10. The image obtained by scanning electron microscopy (SEM) of the chitosan-polypropylene hollow fiber membrane (C-PHF-M) section: **(a)** general section; **(b)** detail of the section highlighting the active layer; and **(c)** detail of the polypropylene hollow fiber membrane (PHF-M) substrate.

3.3. Electrolysis of tungsten electrodes for the recovery of thorium and tungsten

The raw material required for the hybrid thorium recovery process is the remains and ends of the welding electrodes at high temperatures. These materials can be selectively collected on construction sites or industrial production halls and undergo membrane electrolysis followed by nanofiltration, when thorium is recovered as thorium dioxide and tungsten as a tungstate solution.

3.3.1. SEM and EDAX analysis of welding electrodes

The SEM and EDAX characterization of the raw material, the welding electrodes, used in this work highlighted the morphology, but also the surprising composition (Figures 11 and 12). Macroscopically, the welding electrode has a relatively smooth surface (Figure 11a), but with high probability, tungsten filaments appear in the section (Figure 11b), joined by thorium dioxide cubes (Figures 11c and 11d).



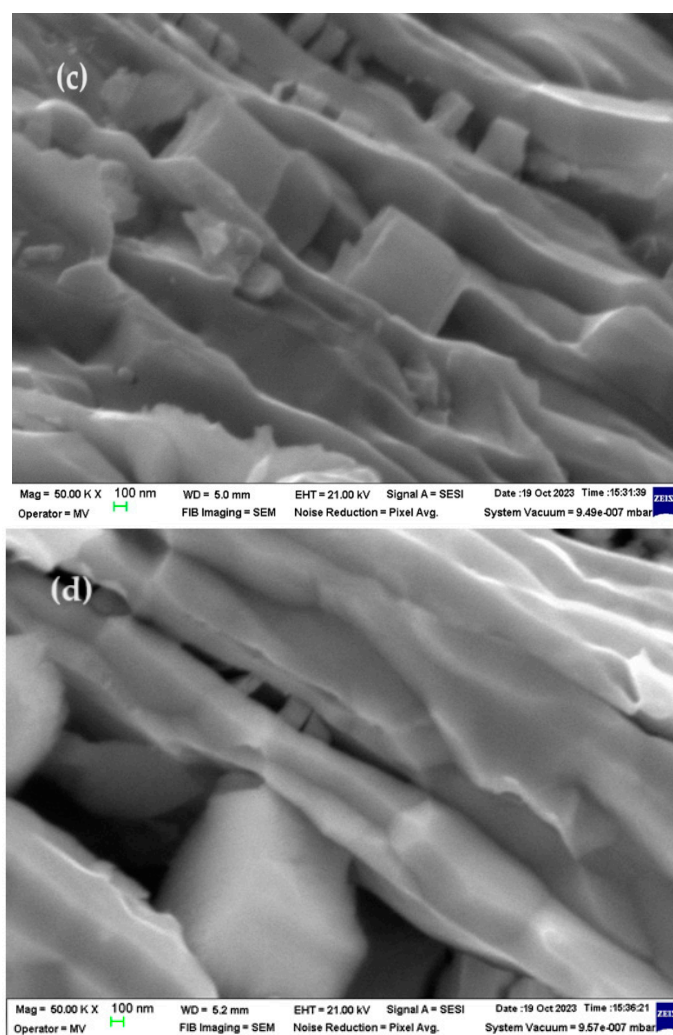


Figure 11. Images obtained by scanning electron microscopy (SEM) for: **(a)** electrode surface; **(b)** the section of the electrode 20,000 \times ; **(c)** the section of the electrode 50,000 \times ; and **(d)** the detail at the electrode section 50,000 \times .

In order to confirm the assessments made by analyzing the electron microscopy, the Energy Dispersive X-ray Spectroscopy (EDAX) analysis was performed in the electrode fracture (Figure 12). Surprisingly (Figures 12 a and b), apart from tungsten, thorium and oxygen appear in the fracture, as well as a measurable amount of aluminum.

The elemental distribution (Figures 12c, 12d and 12f) confirms the assumption that tungsten forms filaments and plates that are joined with nanometric cubes of thorium dioxide. Aluminum, which is distributed over the entire fracture surface of the electrode (Figure 12f), mainly covers the tungsten filaments and plates, suggesting that it is an element with a binding role. The quantitative composition (Figure 12b) is: W 89.4%; thorium 7.1%; oxygen 2.5% and aluminum 1.0%.

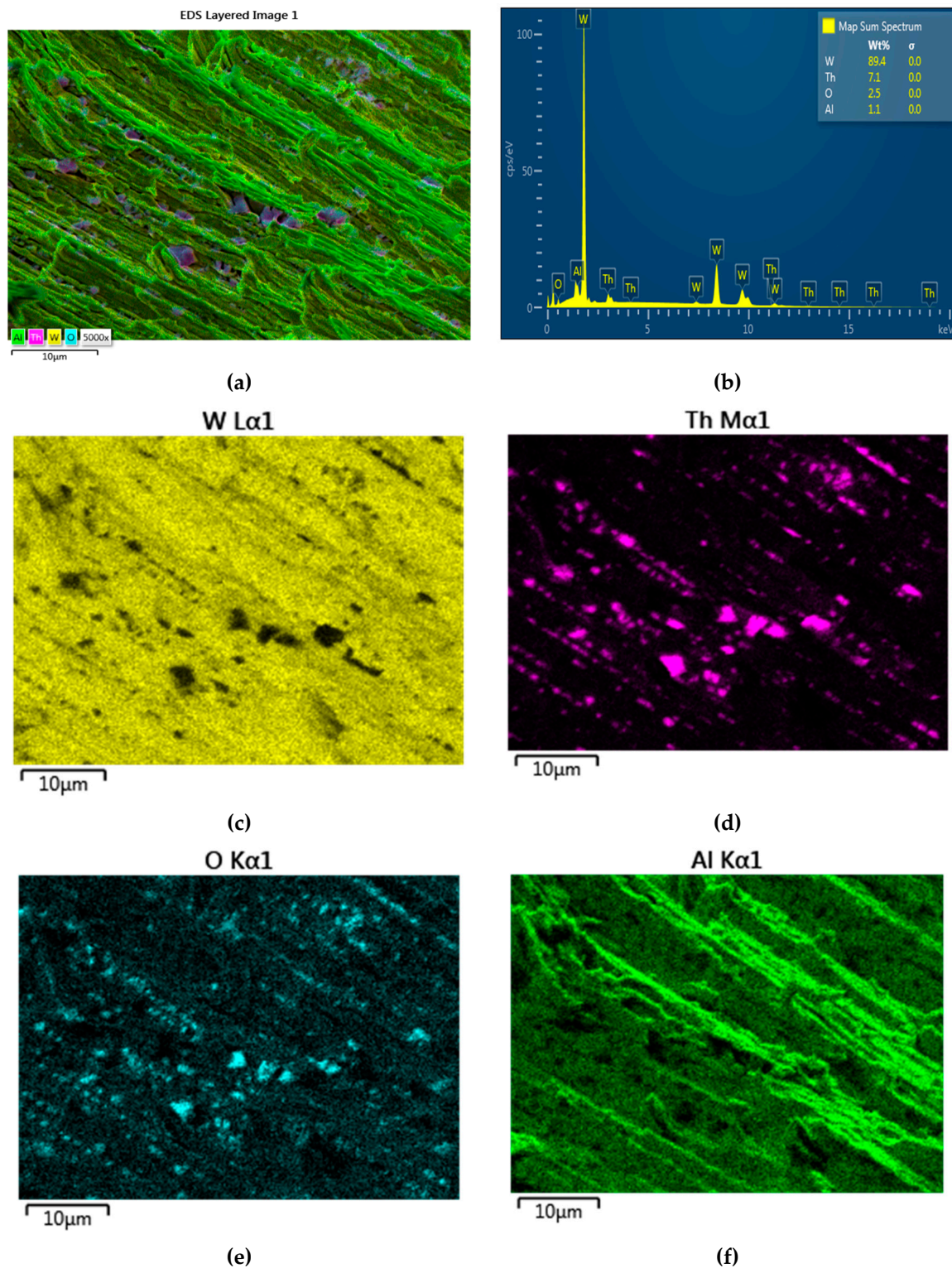


Figure 12. The elemental distribution obtained by Energy Dispersive X-ray Spectroscopy (EDAX) for the fracture of the welding electrode: (a) general distribution of the elements in colors; (b) quantitative elemental composition; (c) tungsten distribution; (d) thorium distribution; (e) oxygen distribution; and (f) aluminum distribution.

3.3.2. Membrane electrolysis of welding electrodes

In order to avoid the loss of thorium as thorium dioxide of nanometric dimensions from the membrane electrolysis process, this was coupled with the nanofiltration of both the solution from the cathode space and the solution in the anode space (Figure 13).

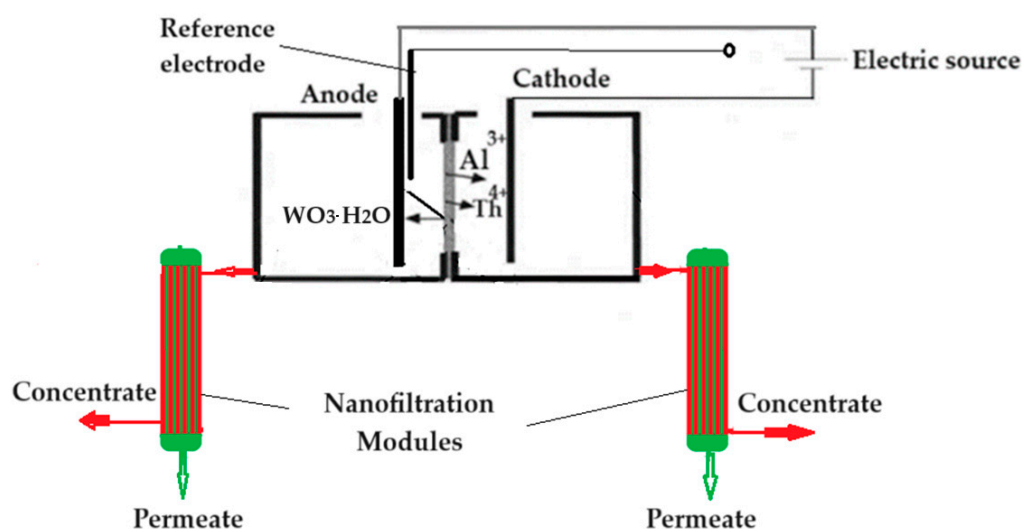
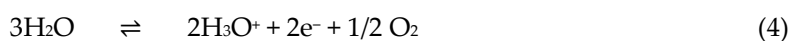
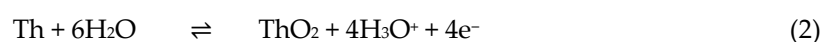
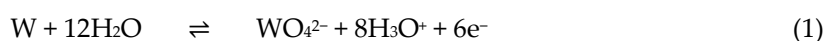


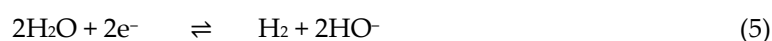
Figure 13. Scheme of the hybrid installation for membrane electrolysis and nanofiltration of tungsten electrodes.

The probable reactions in the anodic space (1–4) and cathodic space (5,6) follow:

ANODE



CATHODE



However, the choice of the potential of the working electrode (anode) as well as the pH in the anodic space largely determine the speciation of each component element of the welding electrodes considered in this study: tungsten, thorium and aluminum (Table 2 and Figure 14). Thus, superimposing the Pourbaix diagrams [61–63] of the three elements (Figure 14) it is possible to specify, at constant potential, the chemical species for each pH in the anodic space (Table 2).

At the potential of 20.0 V and pH=0 in the anodic space, and pH=13 in the cathodic space, following electrolysis, tungsten will be found in the form of tungstic acid $\text{WO}_3 \cdot \text{H}_2\text{O}(\text{s})$, thorium as $\text{Th}^{4+}(\text{aq})$ and aluminum as $\text{Al}^{3+}(\text{aq})$ (Figure 14). The two cations, Th^{4+} and Al^{3+} , will migrate to the cathode, and the tungstic acid will remain in the anodic space. Tungsten in the anode space will be recovered by nanofiltration through the module attached to this space. Thorium will be immobilized as a solid in cathode space in the form of thorium dioxide (ThO_2), and the aluminum ion will pass into sodium aluminate (AlO_2^-), soluble. By nanofiltration [64–66] of the solution from the cathode space through the module attached to this space, thorium dioxide will be retained on the membrane (concentrate) and aluminate ion as permeate.

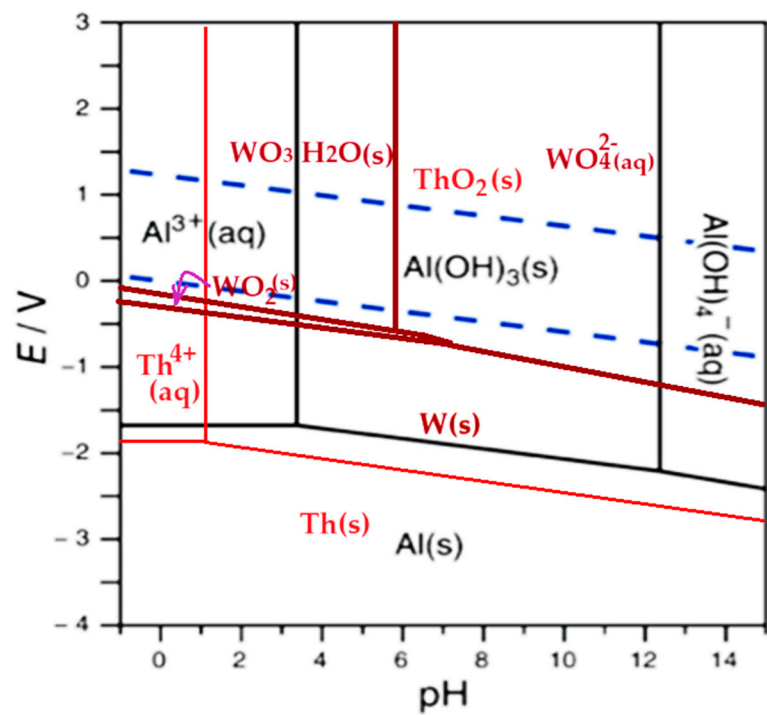


Figure 14. Superimposed Pourbaix diagrams of tungsten (purple), thorium (red), aluminum (black) and the blue dotted lines delimiting the stability domain of water.

At the same potential value of the anodic space, but at pH between 1 and 3.5, the chemical species of the three elements will be: tungsten as $WO_3 \cdot H_2O(s)$, thorium as $ThO_2(s)$, and aluminum as $Al^{3+}(aq)$. In this case, the solution in the anodic space is nanofiltered after treatment with ammonia solution, when ammonium tungstate will pass into the permeate, and thorium dioxide remains on the membrane, in concentrate. The solution in the cathode space will contain sodium aluminate, which, being in solution, does not require nanofiltration. However, for the safety of the hybrid process, the solution from the cathode space also undergoes nanofiltration, when we will find sodium aluminate in the permeate, and any other solid impurity is retained on the membrane.

Table 2. The speciation of tungsten, thorium and aluminum elements depending on the potential and the variable pH in the anodic space, and pH 13 in the cathodic space.

Metallic element or group	Metal element speciation at variable pH in the anodic space, at pH 13 in the cathodic space and 20.0 V anodic potential				
	0–1	1–3	3–6	6–12	>12
Wolfram	$WO_3 \cdot H_2O(s)$	$WO_3 \cdot H_2O(s)$	$WO_3 \cdot H_2O(s)$	$WO_4^{2-}(aq)$	$WO_4^{2-}(aq)$
Thorium	$Th^{4+}(aq)$	$ThO_2(s)$	$ThO_2(s)$	$ThO_2(s)$	$ThO_2(s)$
Aluminum	$Al^{3+}(aq)$	$Al^{3+}(aq)$	$Al(OH)_3(s)$	$Al(OH)_3(s)$	$AlO_2^-(aq)$
sPEEK–M *)	HSO_3-Ar	HSO_3-Ar	$-SO_3-Ar$	$-SO_3-Ar$	$-SO_3-Ar$
C–PHF–M **)	$+H_3N-R$	$+H_3N-R$	$+H_3N-R$	H_2N-R	H_2N-R

*) Ar – aromatic group; **) R – alkyl group.

If the anode has a potential of 20.0 V and the pH in anodic space stays between 3.5 and 6, the chemical species obtained for the three elements are: tungsten as $WO_3 \cdot H_2O(s)$, thorium as $ThO_2(s)$, and aluminum as $Al(OH)_3(s)$. In this case, the solutions from the anodic and cathodic spaces obtained after electrolysis are mixed together and subjected to nanofiltration, when thorium dioxide is retained in the concentrate, and the tungstate and aluminate ions are found in the permeate. To separate the two anions, the pH is adjusted to 5 when the aluminum hydroxide precipitates, which is retained by nanofiltration in the second module of the installation.

If the anode has a potential of 20.0 V, and the pH in the anodic space is kept between 6 and 12, then the chemical species obtained for the three elements are: tungsten as $\text{WO}_4^{2-}(\text{aq})$, thorium as $\text{ThO}_2(\text{s})$, and aluminum as $\text{Al}(\text{OH})_3(\text{s})$.

In this case, the nanofiltration of the anodic space takes place in two stages:

- the first stage at the pH (6–12) from this space when a permeate, containing the soluble tungstate ion, and a concentrate containing thorium dioxide and aluminum hydroxide, are obtained;
- the second stage when the concentrate is mixed with the pH 13 solution from the cathodic space, when the aluminum is solubilized as aluminate, passing into the permeate, and thorium dioxide remains in the concentrate.

If the anode has a potential of 20.0 V, and the pH in the anodic space is above 12, then the chemical species obtained for the three elements are: tungsten as $\text{WO}_4^{2-}(\text{aq})$, thorium as $\text{ThO}_2(\text{s})$ and aluminum as $\text{AlO}_2^-(\text{aq})$.

In this case the nanofiltration of anodic space takes place in two stages:

- the first stage at the pH in this space (above 12), when a permeate containing soluble tungstate and aluminate ions is obtained, and a concentrate containing thorium dioxide and aluminum hydroxide;
- the second stage when the permeate is brought to a pH between 6 and 9, when the aluminum precipitates as hydroxide and is separated from the tungstate ion by nanofiltration, in the second module.

Tungsten recovery after electrolysis means nanofiltration of the solution in order to purify it, because it is obtained as tungstate either by neutralizing tungstic acid or directly, at a pH higher than 6.

The recovery of thorium requires additional attention, firstly because thorium is a radioactive element, and secondly because being obtained as a thorium dioxide dispersion, it will have to be nanofiltered under optimal conditions so as not to be lost in the permeate.

The results obtained during the nanofiltration of nanodispersions, containing thorium dioxide, depending on the pH and at 8 bar working pressure, show flows between 8.5 and 14 $\text{L}/\text{m}^2\cdot\text{h}$ and a removal of thorium reaching below 1 ppm in the permeate, at pH higher than 4, with a determination error of ± 0.1 ppm (Figure 15). This concentration of thorium is below the natural background in various locations in the world, especially those where rare earths are also found [67–73].

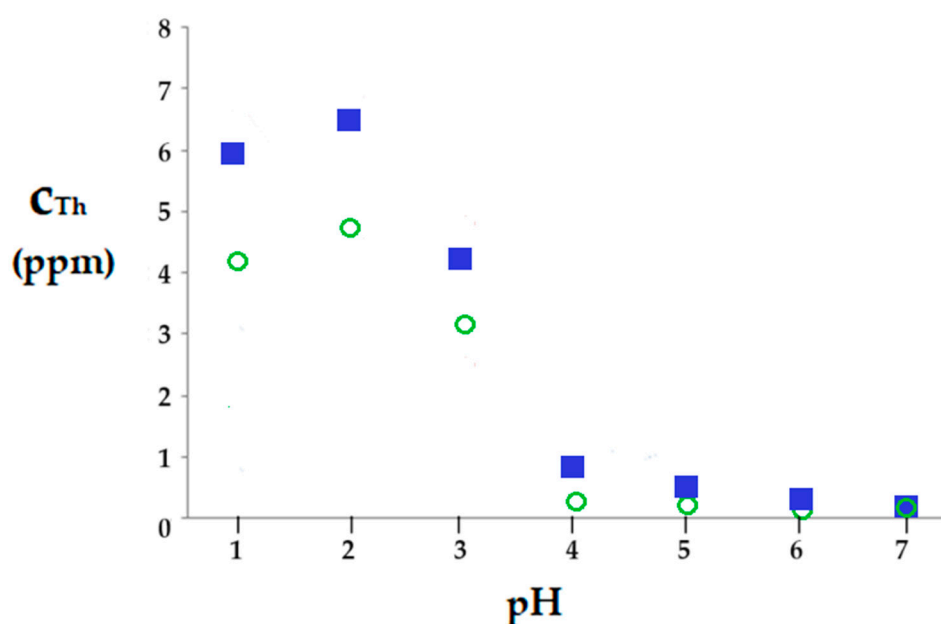


Figure 15. Variation of thorium concentration in the permeate during nanofiltration of thorium dioxide nanodispersion, depending on pH: (blue): thorium dioxide obtained from the electrolysis

process of the welding electrode; and (green) thorium dioxide obtained by precipitation from the solution.

The higher concentration of thorium in the permeate at pH below 3 is due to the existence of thorium dioxide in dispersion and as Th^{4+} ion, which is partially retained by the C-PHF-M membrane, which is in cationic form ($^+\text{H}_3\text{N}-\text{R}$). At pH above 3, the concentration of thorium in the permeate drops sharply to 0.1 ppm, which shows that thorium is found almost entirely as thorium dioxide ThO_2 , and any thorium ions are retained by the membrane in cationic form.

What is interesting is the evolution of the permeate concentration during nanofiltration depending on the morphological nature of thorium dioxide (Figure 14). Thus, over the entire pH range, the concentration of thorium in the permeate for thorium dioxide obtained from electrolysis (Figure 15 – green circles) is lower than that of the same element precipitated from $\text{Th}(\text{NO}_3)_4$ solution (Figure 15 – blue squares).

There can be two reasons for this behavior:

- the existence of thorium in ionic form and as thorium dioxide of different morphology (Figure 16);
- ionic charge of the nanofiltration membrane.

The first argument would probably have a greater influence on the thorium concentration in the permeate. Thus, the thorium dioxide obtained by the precipitation of $\text{Th}(\text{NO}_3)_4$ in amorphous form (Figure 16a) is retained to a lesser extent on the membrane, than the crystalline form of thorium dioxide released from the interstices of the tungsten wires (plates), through electrolysis of the welding electrode (Figures 16b, 11c and 11d).

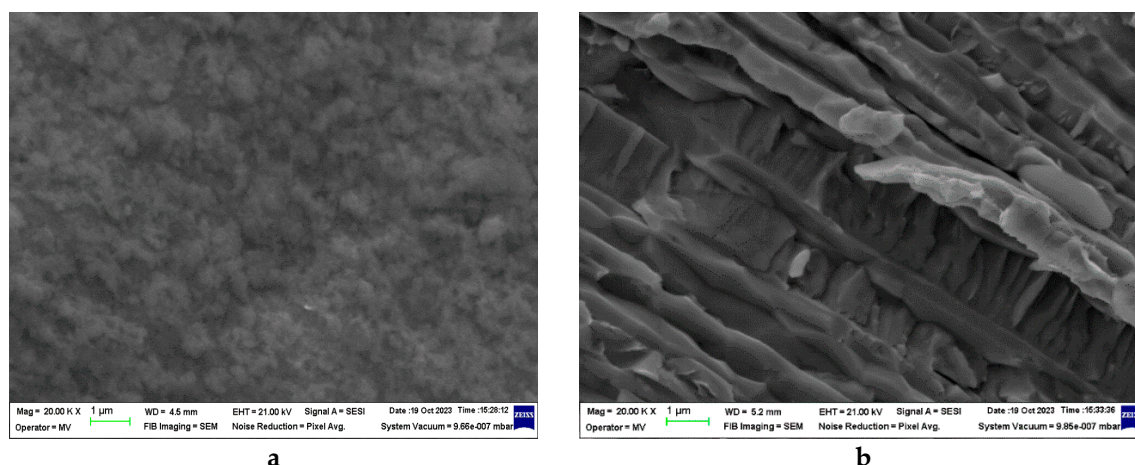


Figure 16. The morphological aspect highlighted through scanning electron microscopy (SEM) for thorium dioxide obtained by: **(a)** precipitation of $\text{Th}(\text{NO}_3)_4$; **(b)** electrolysis of the welding electrode.

The permeate flow performances of nanofiltration of thorium dioxide nanodispersions, from the complex system obtained by electrolysis, depending on pH and working pressure, are presented in Figure 17.

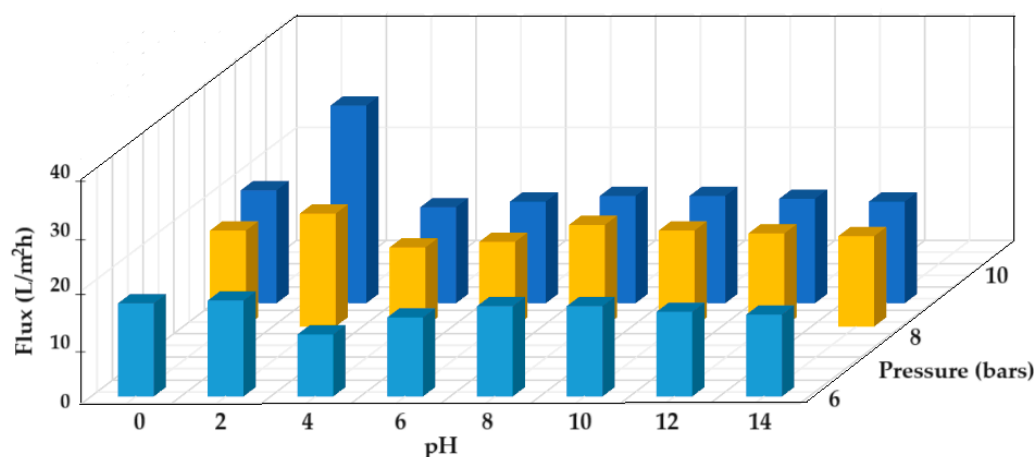


Figure 17. Variation of the nanofiltration flow of nanodispersions containing thorium dioxide, depending on pH and the working pressure.

Over the entire pH range (Figure 17) the fluxes increase with increasing operating pressure from 6 to 10 bar. Each time, from pH 0 to 2, the values of the permeate flows increase up to about 30 L/m²h which is obtained at 10 bars. Starting at pH 4, the flow values increase slightly until pH 10, after which there is a slight decrease.

The recorded flux results are consistent with the speciation of thorium and of the C-PHF-M membrane. At low pH, below 2, thorium is found as ion, and after pH 2 thorium dioxide is formed. It is likely that the size of thorium dioxide nanoparticles increases with the pH, which improves filterability. However, after pH 8 the viscosity of the alkaline solution causes a slight decrease in the permeate flow.

From the point of view of the nanofiltration results, the pH in the electrolysis installation can be up to 2, when we have thorium ions and tungstic acid in the solution, or between 8 and 10 when we have thorium dioxide and tungstate ions in the solution.

The presence of aluminum in the system, even in traces, could impose electrolysis with the anodic space at strongly alkaline pH when aluminum is found as aluminate, tungsten as tungstate, both in solution, and thorium as insoluble precipitated of thorium dioxide. In the latter case, the separation of the anodic and cathodic spaces through the sPEEK membrane becomes unnecessary, the recovery of thorium dioxide being done through a first nanofiltration. The separation of aluminum is done by the second nanofiltration, after adjusting the pH between 5 and 9 when the aluminum will be retained on the membrane in the form of insoluble aluminum hydroxide.

4. Conclusions

The recovery and recycling of metals that generate toxic ions in the environment is of particular importance, especially when these are tungsten, aluminum and, above all, thorium.

This paper presents the separation and recovery of tungsten, thorium and aluminum from welding electrodes at high temperature, in a hybrid installation of membrane electrolysis and nanofiltration. The membranes used are made from sPEEK for the separation of anodic and cathodic spaces in the electrolysis cell, and from chitosan deposited on polypropylene hollow fiber membrane (C-PHF-M) in the nanofiltration module.

Through electrolysis at 20.0 V and variable pH, the speciation of the three studied elements could be separated. Favorable conditions for both electrolysis and nanofiltration were obtained at pH from 6 to 9 when the soluble tungstate ion, solid aluminum hydroxide and solid thorium dioxide were formed. Through a first nanofiltration, the tungstate ion is obtained in the permeate, and thorium dioxide and aluminum hydroxide in the concentrate. By adding a pH 13 solution over the two precipitates, aluminum is solubilized as soluble sodium aluminate, which after the second nanofiltration will be found in the permeate, the thorium dioxide remaining integral (within an error of ± 0.1 ppm) on the C-PHF-M membrane.

Variants of the operation procedure of the hybrid electrolysis and nanofiltration installation were suggested by superimposing the Pourbaix diagrams of tungsten, thorium and aluminum.

The increase of the working potential above the value of 20.0 V brings only the increase of molecular oxygen in the anodic space as a chemical speciation modification.

Author Contributions: Conceptualization, G.T.M., G.N., and V.-A.G.; methodology, A.C.N., A.R.G. and D.I.P.; validation, D.I.P., V.E.M., and A.R.G.; formal analysis, A.C.N., A.R.G. and D.I.P.; investigation, G.T.M., G.N., V.E.M., P.C.A., V.-A.G.; A.C.N., A.R.G. and D.I.P.; resources, G.T.M., G.N., D.I.P. and, P.C.A.; data curation, A.C.N., A.R.G., V.-A.G. writing—original draft preparation, G.T.M., G.N., A.C.N. and, V.-A.G.; writing—review and editing, G.T.M., G.N., and V.-A.G. All authors have read and agreed to the published version of the manuscript.

Funding: Part of this research was conducted under Program 1 – *Development of the national research and development system*, Subprogram 1.1. *Institutional performance – Projects to finance excellence in RDI*, Contract No. 19PFE/12.30.2021, funded by the Ministry of Research, Innovation and Digitization (for the work of Geani Teodor Man and Diana Ionela Popescu (Stegarus)). The partial financial support was provided by the Ministry of Research, Innovation and Digitization through contract PN 23140201/42N-2023 (for the work of Virgil Emanuel Marinescu). The partial financial support was provided by the Ministry of Research, Innovation and Digitization through contract PN 21 02 03 (for the work of Paul Constantin Albu).

Institutional Review Board Statement: Not applicable.

Informed Consent Statement: Not applicable.

Acknowledgments: The authors gratefully acknowledge the valuable help and friendly assistance of Eng. Roxana Truşcă for performing the membrane scanning microscopy analysis.

Conflicts of Interest: The authors declare no conflict of interest.

References

- Deng, P.; Cheng, L.; Li, A.; Zeng, Z.; Liao, C. Recent Advances in the Utilization of Tungsten Residue: A Mini Review of China. *Metals* **2023**, *13*, 1481. <https://doi.org/10.3390/met13081481>.
- Huang, M.; Hu, K.; Li, X.; Wang, Y.; Ouyang, J.; Zhou, L.; Liu, Z. Mineralogical Properties of a Refractory Tantalum-Niobium Slag and the Effect of Roasting on the Leaching of Uranium-Thorium. *Toxics* **2022**, *10*(8), 469. <https://doi.org/10.3390/toxics10080469>.
- Han, Z.; Golev, A.; Edraki, M. A Review of Tungsten Resources and Potential Extraction from Mine Waste. *Minerals* **2021**, *11*, 701. <https://doi.org/10.3390/min11070701>.
- Mahmoud, A.E.D.; Mostafa, E. Nanofiltration Membranes for the Removal of Heavy Metals from Aqueous Solutions: Preparations and Applications. *Membranes* **2023**, *13*, 789. <https://doi.org/10.3390/membranes13090789>.
- Abdusamadzoda, D.; Abdushukurov, D.A.; Duliu, O.G.; Zinicovscaia, I. Assessment of the Toxic Metals Pollution of Soil and Sediment in Zarafshon Valley, Northwest Tajikistan (Part II). *Toxics* **2020**, *8*, 113. <https://doi.org/10.3390/toxics8040113>.
- Safiulina, A.M.; Lizunov, A.V.; Semenov, A.A.; Baulin, D.V.; Baulin, V.E.; Tsivadze, A.Y.; Aksenov, S.M.; Tananaev, I.G. Recovery of Uranium, Thorium, and Other Rare Metals from Eudialyte Concentrate by a Binary Extractant Based on 1,5-bis[2-(hydroxyethoxyphosphoryl)-4-ethylphenoxy]-3-oxapentane and Methyl Trioctylammonium Nitrate. *Minerals* **2022**, *12*, 1469. <https://doi.org/10.3390/min12111469>.
- Ushakov, S.V.; Hong, Q.-J.; Gilbert, D.A.; Navrotsky, A.; Walle, A.v.d. Thorium and Rare Earth Monoxides and Related Phases. *Materials* **2023**, *16*, 1350. <https://doi.org/10.3390/ma16041350>.
- Kukkonen, E.; Virtanen, E.J.; Moilanen, J.O. α -Aminophosphonates, -Phosphinates, and -Phosphine Oxides as Extraction and Precipitation Agents for Rare Earth Metals, Thorium, and Uranium: A Review. *Molecules* **2022**, *27*, 3465. <https://doi.org/10.3390/molecules27113465>.
- Arabi, H.R.; Milani, S.A.; Abolghasemi, H.; Zahakifar, F. Recovery and transport of thorium (IV) through polymer inclusion membrane with D2EHPA from nitric acid solutions. *Journal of Radioanalytical and Nuclear Chemistry*, **2021**, *327*, pp.653–665.
- Houessionon, M.G.K.; Ouendo, E.-M.D.; Bouland, C.; Takyi, S.A.; Kedote, N.M.; Fayomi, B.; Fobil, J.N.; Basu, N. Environmental Heavy Metal Contamination from Electronic Waste (E-Waste) Recycling Activities Worldwide: A Systematic Review from 2005 to 2017. *Int. J. Environ. Res. Public Health* **2021**, *18*, 3517. <https://doi.org/10.3390/ijerph18073517>.
- Lu, J.; He, K.; Wang, Y.; Chen, G.; Weng, H.; Lin, M. An Effective Process for the Separation of U(VI), Th(IV) from Rare Earth Elements by Using Ionic Liquid Cyphos IL 104. *Chin. Chem. Lett.* **2022**, *33*, 3422–3428. <https://doi.org/10.1016/j.ccllet.2022.03.089>.

12. Man, G.T.; Albu, P.C.; Nechifor, A.C.; Grosu, A.R.; Tanczos, S.-K.; Grosu, V.-A.; Ioan, M.-R.; Nechifor, G. Thorium Removal, Recovery and Recycling: A Membrane Challenge for Urban Mining. *Membranes* **2023**, *13*, 765. <https://doi.org/10.3390/membranes13090765>.
13. Zhang, H.; Gao, Y. Polymeric Materials for Rare Earth Elements Recovery. *Gels* **2023**, *9*, 775. <https://doi.org/10.3390/gels9100775>.
14. Pathapati, S.V.S.H.; Free, M.L.; Sarswat, P.K. A Comparative Study on Recent Developments for Individual Rare Earth Elements Separation. *Processes* **2023**, *11*, 2070. <https://doi.org/10.3390/pr11072070>.
15. Saleh, T.A.; Sari, A.; Tuzen, M., Development and characterization of bentonite-gum arabic composite as novel highly-efficient adsorbent to remove thorium ions from aqueous media. *Cellulose*, **2021**, *28*, 10321-10333. <https://doi.org/10.1007/s10570-021-04158-1>.
16. Ault, T.; Krahn, S.; Croff, A. Comparing the environmental impacts of uranium- and thorium-based fuel cycles with different recycle options. *Prog. Nucl. Energy* **2017**, *100*, 114–134. <https://doi.org/10.1016/j.pnucene.2017.05.010>.
17. Elbshary, R.E.; Gouda, A.A.; El Sheikh, R.; Alqahtani, M.S.; Hanfi, M.Y.; Atia, B.M.; Sakr, A.K.; Gado, M.A. Recovery of W(VI) from Wolframite Ore Using New Synthetic Schiff Base Derivative. *Int. J. Mol. Sci.* **2023**, *24*, 7423. <https://doi.org/10.3390/ijms24087423>.
18. Xu, L.; Zhao, B. Extraction of Sodium Tungstate from Tungsten Ore by Pyrometallurgical Smelting. *Metals* **2023**, *13*, 312. <https://doi.org/10.3390/met13020312>.
19. Kumar, R.; Kariminejad, A.; Antonov, M.; Goljandin, D.; Klimczyk, P.; Hussainova, I. Progress in Sustainable Recycling and Circular Economy of Tungsten Carbide Hard Metal Scraps for Industry 5.0 and Onwards. *Sustainability* **2023**, *15*, 12249. <https://doi.org/10.3390/su151612249>.
20. Han, Z.; Golev, A.; Edraki, M. A Review of Tungsten Resources and Potential Extraction from Mine Waste. *Minerals* **2021**, *11*, 701. <https://doi.org/10.3390/min11070701>.
21. Katiyar, P.K.; Randhawa, N.S. A comprehensive review on recycling methods for cemented tungsten carbide scraps highlighting the electrochemical techniques. *Int. J. Refract. Met. Hard Mater.* **2020**, *90*, 105251. <https://doi.org/10.1016/j.jrmhm.2020.105251>.
22. Das, S.K.; Nagesh, C.H.R.V.S.; Sreenivas, T.; Kundu, T.; Angadi, S.I. A treatise on occurrence, beneficiation and plant practices of tungsten-bearing ores. *Powder Technology* **2023**, *429*, 118938. <https://doi.org/10.1016/j.powtec.2023.118938>.
23. Sabbatovskii, K.G.; The effect of the adsorption of multicharge cations on the selectivity of a nanofiltration membrane. *Colloid J.* **2003**, *65*, 237–243. <https://doi.org/10.1023/A:1023333628708>.
24. Kaptakov, V.O.; Milyutin, V.V.; Nekrasova, N.A.; Zelenin, P.G.; Kozlitsin, E.A. Nanofiltration Extraction of Uranium and Thorium from Aqueous Solutions. *Radiochemistry* **2021**, *63*, 169–172. <https://doi.org/10.1134/S1066362221020065>.
25. Ilaiyaraja, P.; Deb, A.K.S.; Ponraju, D. Removal of uranium and thorium from aqueous solution by ultrafiltration (UF) and PAMAM dendrimer assisted ultrafiltration (DAUF). *Journal of Radioanalytical and Nuclear Chemistry*, **2015**, *303*, 441-450.
26. Katiyar, P.K.; Randhawa, N.S.; Hait, J.; Jana, R.K.; Singh, K.K.; Mankhand, T.R. Anodic Dissolution Behaviour of Tungsten Carbide Scraps in Ammoniacal Media. *Adv. Mater. Res.* **2014**, *828*, 11–20. <https://doi.org/10.4028/www.scientific.net/AMR.828.11>.
27. Kuntiy, O.I.; Ivashkin, V.R.; Yavorskii, V.T.; Zozulya, G.I. Electrochemical processing of WC-Ni pseudoalloys in sulfuric acid solutions to ammonium paratungstate and nickel(II) sulfate. *Russ. J. Appl. Chem.* **2007**, *80*, 1856–1859. <https://doi.org/10.1134/S1070427207110158>.
28. Ubaldini, A.; Cicconi, F.; Rizzo, A.; Salvi, S.; Cuzzola, V.; Gennerini, F.; Bruni, S.; Marghella, G.; Gessi, A.; Falsini, N. Preparation and Characterization of Isostructural Na₂MoO₄ and Na₂WO₄ and a Study of the Composition of Their Mixed System. *Molecules* **2023**, *28*, 6602. <https://doi.org/10.3390/molecules28186602>.
29. Liu, H.; Liu, H.; Nie, C.; Zhang, J.; Steenari, B.M.; Ekberg, C. Comprehensive treatments of tungsten slags in China: A critical review. *Journal of Environmental Management*, **2020**, *270*, p.110927. <https://doi.org/10.1016/j.jenvman.2020.110927>.
30. Cao, Y.; Guo, Q.; Sun, W.; Chelnokov, G.A. Efficient and Fast Removal of Aqueous Tungstate by an Iron-Based LDH Delaminated in L-Asparagine. *Int. J. Environ. Res. Public Health* **2022**, *19*, 7280. <https://doi.org/10.3390/ijerph19127280>.
31. Leal Filho, W.; Kotter, R.; Özuyar, P.G.; Abubakar, I.R.; Eustachio, J.H.P.P.; Matandirotya, N.R. Understanding Rare Earth Elements as Critical Raw Materials. *Sustainability* **2023**, *15*, 1919. <https://doi.org/10.3390/su15031919>.
32. Aziman, E.S.; Mohd Salehuddin, A.H.J.; Ismail, A.F. Remediation of thorium (IV) from wastewater: Current status and way forward. *Separation & Purification Reviews*, **2021**, *50*(2), pp.177-202. <https://doi.org/10.1080/15422119.2019.1639519>.
33. Gomaa, H.; Emran, M.Y.; Elsenety, M.M.; Abdel-Rahim, R.D.; Deng, Q.; Gadallah, M.I.; Saad, M.; AlMohiy, H.; Ezzeldien, M.; Seaf El-Nasr, T.A.; El-Gaby, M.S. Detection and Selective Removal Strategy of Thorium

- Ions Using a Novel Fluorescent Ligand and Hybrid Mesoporous γ -Al₂O₃-like Nanoneedles. *ACS Sustainable Chemistry & Engineering* **2023**, 11(6), 2127-2138. <https://doi.org/10.1021/acssuschemeng.2c05000>.
34. Rahman, I.U.; Mohammed, H.J.; Siddique, M.F.; Ullah, M.; Bamasag, A.; Alqahtani, T; Algarni, S. Application of membrane technology in the treatment of waste liquid containing radioactive materials. *Journal of Radioanalytical and Nuclear Chemistry*, **2023**, 1-14. <https://doi.org/10.1007/s10967-023-09169-9>.
 35. Xiong, L.; Lyu, K.; Zeng, Y.; Yang, C.; Chi, F.; Hu, S.; Long, X. Stable and high-flux polyacrylonitrile/hafnium phosphonate nanofibrous membranes for efficient removal of actinides from strong acidic solutions. *Journal of Environmental Chemical Engineering*, **2023**, 11(2), 109619. <https://doi.org/10.1016/j.jece.2023.109619>.
 36. Abbasizadeh, S.; Keshtkar, A.R.; Mousavian, M.A. Preparation of a novel electrospun polyvinyl alcohol/titanium oxide nanofiber adsorbent modified with mercapto groups for uranium (VI) and thorium (IV) removal from aqueous solution. *Chem. Eng. J.* **2013**, 220, 161–171. <https://doi.org/10.1016/j.cej.2013.01.029>.
 37. Tsezos, M.; Volesky, B. Biosorption of uranium and thorium. *Biotechnol. Bioeng.* **1981**, 23, 583–604. <https://doi.org/10.1002/bit.260230309>.
 38. Hritcu, D.; Humelnicu, D.; Dodi, G.; Popa, M.I. Magnetic chitosan composite particles: Evaluation of thorium and uranyl ion adsorption from aqueous solutions. *Carbohydr. Polym.* **2012**, 87, 1185–1191. <https://doi.org/10.1016/j.carbpol.2011.08.095>.
 39. Zolfonoun, E.; Yousefi, S.R. Sorption and preconcentration of uranium and thorium from aqueous solutions using multi-walled carbon nanotubes decorated with magnetic nanoparticles. *Radiochim. Acta* **2015**, 103, 835–841. <https://doi.org/10.1515/ract-2015-2466>.
 40. Nechifor, A.C.; Goran, A.; Grosu, V.-A.; Bungău, C.; Albu, P.C.; Grosu, A.R.; Oprea, O.; Păncescu, F.M.; Nechifor, G. Improving the Performance of Composite Hollow Fiber Membranes with Magnetic Field Generated Convection Application on pH Correction. *Membranes* **2021**, 11, 445. <https://doi.org/10.3390/membranes11060445>.
 41. Nechifor, G.; Păncescu, F.M.; Grosu, A.R.; Albu, P.C.; Oprea, O.; Tanczos, S.-K.; Bungău, C.; Grosu, V.-A.; Pîrțac, A.; Nechifor, A.C. Osmium Nanoparticles-Polypropylene Hollow Fiber Membranes Applied in Redox Processes. *Nanomaterials* **2021**, 11, 2526. <https://doi.org/10.3390/nano11102526>.
 42. Paun, G.; Neagu, E.; Parvulescu, V.; Anastasescu, M.; Petrescu, S.; Albu, C.; Nechifor, G.; Radu, G.L. New Hybrid Nanofiltration Membranes with Enhanced Flux and Separation Performances Based on Polyphenylene Ether-Ether-Sulfone/Polyacrylonitrile/SBA-15. *Membranes* **2022**, 12, 689. <https://doi.org/10.3390/membranes12070689>.
 43. Cimbru, A.M.; Rikabi, A.A.K.K.; Oprea, O.; Grosu, A.R.; Tanczos, S.-K.; Simonescu, M.C.; Pașcu, D.; Grosu, V.-A.; Dumitru, F.; Nechifor, G. *pH* and *pCl* Operational Parameters in Some Metallic Ions Separation with Composite Chitosan/Sulfonated Polyether Ether Ketone/Polypropylene Hollow Fibers Membranes. *Membranes* **2022**, 12, 833. <https://doi.org/10.3390/membranes12090833>.
 44. Păncescu, F.M.; Rikabi, A.A.K.K.; Oprea, O.C.; Grosu, A.R.; Nechifor, A.C.; Grosu, V.-A.; Tanczos, S.-K.; Dumitru, F.; Nechifor, G.; Bungău, S.G. Chitosan-sEPDM and Melatonin-Chitosan-sEPDM Composite Membranes for Melatonin Transport and Release. *Membranes* **2023**, 13, 282. <https://doi.org/10.3390/membranes13030282>.
 45. Pașcu, D.; Nechifor, A.C.; Grosu, V.-A.; Oprea, O.C.; Tanczos, S.-K.; Man, G.T.; Dumitru, F.; Grosu, A.R.; Nechifor, G. Hydrogen Sulphide Sequestration with Metallic Ions in Acidic Media Based on Chitosan/sEPDM/Polypropylene Composites Hollow Fiber Membranes System. *Membranes* **2023**, 13, 350. <https://doi.org/10.3390/membranes13030350>.
 46. Dimulescu, I.A.; Nechifor, A.C.; Bărdacă, C.; Oprea, O.; Pașcu, D.; Totu, E.E.; Albu, P.C.; Nechifor, G.; Bungău, S.G. Accessible Silver-Iron Oxide Nanoparticles as a Nanomaterial for Supported Liquid Membranes. *Nanomaterials* **2021**, 11, 1204. <https://doi.org/10.3390/nano11051204>.
 47. Nechifor, A.C.; Cotorcea, S.; Bungău, C.; Albu, P.C.; Pașcu, D.; Oprea, O.; Grosu, A.R.; Pîrțac, A.; Nechifor, G. Removing of the Sulfur Compounds by Impregnated Polypropylene Fibers with Silver Nanoparticles-Cellulose Derivatives for Air Odor Correction. *Membranes* **2021**, 11, 256. <https://doi.org/10.3390/membranes11040256>.
 48. Nechifor, G.; Păncescu, F.M.; Grosu, A.R.; Albu, P.C.; Oprea, O.; Tanczos, S.-K.; Bungău, C.; Grosu, V.-A.; Pîrțac, A.; Nechifor, A.C. Osmium Nanoparticles-Polypropylene Hollow Fiber Membranes Applied in Redox Processes. *Nanomaterials* **2021**, 11, 2526. <https://doi.org/10.3390/nano11102526>.
 49. Bărdacă Urducea, C.; Nechifor, A.C.; Dimulescu, I.A.; Oprea, O.; Nechifor, G.; Totu, E.E.; Isildak, I.; Albu, P.C.; Bungău, S.G. Control of Nanostructured Polysulfone Membrane Preparation by Phase Inversion Method. *Nanomaterials* **2020**, 10, 2349. <https://doi.org/10.3390/nano10122349>.
 50. Pavel, E.; Prodan, G.; Marinescu, V.; Trusca, R. Recent advances in 3- to 10-nm quantum optical lithography. *Journal of Micro/Nanolithography, MEMS, and MOEMS* **2019**, 18(2), 020501 (7 May). <https://doi.org/10.1117/1.JMM.18.2.020501>.

51. Prioteasa, P.; Marinescu, V.; Bara, A.; Iordoc, M.; Teisanu, A.; Banciu, C.; Meltzer, V. Electrodeposition of Polypyrrole on Carbon Nanotubes/Si in the Presence of Fe Catalyst for Application in Supercapacitors. *Rev. Chim.* **2015**, *66*, 820-824.
52. Zamfir, L.-G.; Rotariu, L.; Marinescu, V. E.; Simelane, X.T.; Baker, P.G.L.; Iwuoha, E. I.; Bala, C. Non-enzymatic polyamic acid sensors for hydrogen peroxide detection. *Sensors and Actuators B: Chemical*, **2016**, *226*, 525-533. <https://doi.org/10.1016/j.snb.2015.12.026>.
53. Cazalaà, J.B. Radium and thorium applications for the general public: unexpected consequences of the discovery from Pierre and Marie Curie. *The Journal of the American Society of Anesthesiologists* **2012**, *117*(6), 1202-1202. <https://doi.org/10.1097/ALN.0b013e31827ce176>.
54. Pohjalainen, I.; Moore, I.D.; Geldhof, S.; Rosecker, V.; Sterba, J.; Schumm, T. Gas cell studies of thorium using filament dispensers at IGISOL. *Nuclear Instruments and Methods in Physics Research Section B: Beam Interactions with Materials and Atoms* **2020**, *484*, 59-70, <https://doi.org/10.1016/j.nimb.2020.08.012>.
55. Takaki, N.; Mardiansah, D. Core Design and Deployment Strategy of Heavy Water Cooled Sustainable Thorium Reactor. *Sustainability* **2012**, *4*, 1933-1945. <https://doi.org/10.3390/su4081933>.
56. Sidik, P.; Takaki, N.; Sekimoto, H. Feasible region of design parameters for water cooled thorium breeder reactor. *J. Nucl. Sci. Technol.* **2007**, *44*, 946-957. <https://doi.org/10.1080/18811248.2007.9711334>.
57. Aranaz, I.; Alcántara, A.R.; Civera, M.C.; Arias, C.; Elorza, B.; Heras Caballero, A.; Acosta, N. Chitosan: An Overview of Its Properties and Applications. *Polymers* **2021**, *13*, 3256. <https://doi.org/10.3390/polym13193256>.
58. Jiménez-Gómez, C.P.; Cecilia, J.A. Chitosan: A Natural Biopolymer with a Wide and Varied Range of Applications. *Molecules* **2020**, *25*, 3981. <https://doi.org/10.3390/molecules25173981>.
59. Ibrahim, M.A.; Alhalafi, M.H.; Emam, E.-A.M.; Ibrahim, H.; Mosaad, R.M. A Review of Chitosan and Chitosan Nanofiber: Preparation, Characterization, and Its Potential Applications. *Polymers* **2023**, *15*, 2820. <https://doi.org/10.3390/polym15132820>.
60. Radu, E.-R.; Pandele, A.M.; Tuncel, C.; Miculescu, F.; Voicu, S.I. Preparation and Characterization of Chitosan/LDH Composite Membranes for Drug Delivery Application. *Membranes* **2023**, *13*, 179. <https://doi.org/10.3390/membranes13020179>.
61. Nave, M.I.; Kornev, K.G. Complexity of Products of Tungsten Corrosion: Comparison of the 3D Pourbaix Diagrams with the Experimental Data. *Metall. Mater. Trans. A* **2017**, *48*, 1414-1424. <https://doi.org/10.1007/s11661-016-3888-6>.
62. Berlanga-Labari, C.; Biezma-Moraleda, M.V.; Rivero, P.J. Corrosion of Cast Aluminum Alloys: A Review. *Metals* **2020**, *10*(10), 1384. <https://doi.org/10.3390/met10101384>.
63. Han, K.N. Characteristics of Precipitation of Rare Earth Elements with Various Precipitants. *Minerals* **2020**, *10*, 178. <https://doi.org/10.3390/min10020178>.
64. Ma, H.; Shen, M.; Tong, Y.; Wang, X. Radioactive Wastewater Treatment Technologies: A Review. *Molecules* **2023**, *28*, 1935. <https://doi.org/10.3390/molecules28041935>.
65. Rybak, A.; Rybak, A. Characteristics of Some Selected Methods of Rare Earth Elements Recovery from Coal Fly Ashes. *Metals* **2021**, *11*, 142. <https://doi.org/10.3390/met11010142>.
66. Chang, H.; Zhang, G. Separation Techniques for the Efficient and Green Recovery of Metal Minerals. *Separations* **2023**, *10*, 520. <https://doi.org/10.3390/separations10100520>.
67. Nisbet, H.; Migdisov, A.; Xu, H.; Guo, X.; van Hinsberg, V.; Williams-Jones, A.E.; Boukhalfa, H.; Roback, R. An experimental study of the solubility and speciation of thorium in chloride-bearing aqueous solutions at temperatures up to 250 °C. *Geochimica et Cosmochimica Acta* **2018**, *239*, 363-373. <https://doi.org/10.1016/j.gca.2018.08.001>.
68. Kusumkar, V.V.; Galamboš, M.; Viglašová, E.; Daño, M.; Šmelková, J. Ion-Imprinted Polymers: Synthesis, Characterization, and Adsorption of Radionuclides. *Materials* **2021**, *14*, 1083. <https://doi.org/10.3390/ma14051083>.
69. Atanassova, M. Thenoyltrifluoroacetone: Preferable Molecule for Solvent Extraction of Metals—Ancient Twists to New Approaches. *Separations* **2022**, *9*, 154. <https://doi.org/10.3390/separations9060154>.
70. Peng, C.; Ma, Y.; Ding, Y.; He, X.; Zhang, P.; Lan, T.; Wang, D.; Zhang, Z.; Zhang, Z. Influence of Speciation of Thorium on Toxic Effects to Green Algae *Chlorella pyrenoidosa*. *Int. J. Mol. Sci.* **2017**, *18*, 795. <https://doi.org/10.3390/ijms18040795>.
71. Vakanjac, B.; Naunovic, Z.; Ristić Vakanjac, V.; Đumić, T.; Bakrač, S.; Štrbački, J.; Gajić, V.; Alzarog, T.M. Distribution of Potentially Toxic Elements in the City of Zintan and Its Surroundings (Northwestern Libya) by Surface Soil Sampling. *Minerals* **2023**, *13*, 1048. <https://doi.org/10.3390/min13081048>.
72. García, A.C.; Latifi, M.; Amini, A.; Chaouki, J. Separation of Radioactive Elements from Rare Earth Element-Bearing Minerals. *Metals* **2020**, *10*, 1524. <https://doi.org/10.3390/met10111524>.
73. Kaptakova, V.O.; Milyutina, V.V.; Nekrasovaa, N.A.; Zelenina, P.G.; Kozlitina, E.A.; Nanofiltration Extraction of Uranium and Thorium from Aqueous Solutions. *Radiochemistry*, **2021**, *63*(2), 169-172. ISSN 1066-3622, © Pleiades Publishing, Inc., **2021**. Russian Text © The Author(s), **2021**, published in *Radiokhimiya*, **2021**, *63*(2), 139-142.

Disclaimer/Publisher's Note: The statements, opinions and data contained in all publications are solely those of the individual author(s) and contributor(s) and not of MDPI and/or the editor(s). MDPI and/or the editor(s) disclaim responsibility for any injury to people or property resulting from any ideas, methods, instructions or products referred to in the content.